

Electrodeposition of Large Area, Angle-Insensitive Multilayered Structural Colors

Chengang Ji,^{1,†} Saurabh Acharya,^{1,†} Kaito Yamada,² Stephen Maldonado,^{2,3,*} and L. Jay Guo^{1,2,*}

¹Department of Electrical Engineering and Computer Science, ²Applied Physics Program, ³Department of Chemistry, The University of Michigan, Ann Arbor, Michigan 48109, USA

Abstract: We demonstrate structural colors produced by a simple, inexpensive, and non-toxic electrochemical process. Asymmetric metal-dielectric-metal multilayered structures were achieved by sequential electrodeposition of smooth gold, thin cuprous oxide, and finally thin Au on conductive substrates, forming an effective optical cavity with angle-insensitive characteristics. Different colors of high brightness were achieved by simply tuning the thickness of the electrodeposited middle cavity layer. This process is compatible with highly non-planar substrates of arbitrary shape, size and roughness. This work is the first demonstration of solution-processed, electrodeposited metal-dielectric-metal film stacks and highlights the clear advantages of this approach over traditional deposition or assembly methods for preparing colored films.

Keywords: structural colors; electrodeposition; nanocavities; thin films; angular insensitivity.

Introduction

Color filters that selectively transmit or reflect visible light are highly desired in a wide variety of applications, including optical displays,^{1,2} colored printings,³⁻⁵ aesthetic decorations,^{6,7} and energy harvesting.⁸⁻¹³ Structural colors based on optical resonance effect have attracted much attention. As compared with traditional colorant-based pigmentations, structural colors offer the advantage of high brightness, ultra-compactness, easy manufacturability, and long-term stability.¹⁴ Many schemes based on plasmonic or guide-mode resonances have been proposed for color generation.^{4,15-18} However, most of the structural colors demonstrated to date involve complex patterns or expensive fabrication processes, which limits high volume production. In comparison simple 1D layered structural colors made by vacuum deposition provide one possible approach for mass-production.^{7, 19-21} Roll-to-roll vacuum deposition methods have been developed for obtaining pigment flakes exhibiting unique metallic appearance with high purity for decorative paints and colored solar cells,²² however these methods carry a high cost associated with having to rely on vacuum deposition systems.

Approaches that produce high quality thin-films at ambient conditions are thus highly desirable. Three-dimensional (3D) photonic crystals employing self-assembled nanoparticles to generate colors have been explored.²³⁻²⁸ However, the color properties of pigment flakes made by nanoparticle assemblies for decorative paints are compromised by disorder and disassembly during the necessary grinding steps to obtain dispersible flakes.

In comparison, electrochemical methods can be simultaneously performed under mild conditions and with the unique advantage of being applicable to objects of arbitrary shape and size. Electrodeposition specifically affords conformal film coatings on substrates with both micro- and macro- roughness²⁹⁻³¹ since film nucleation^{32, 33} and growth rate are readily controllable in real-time by regulation of the applied potential/current.

In this work, we present data describing a simple and inexpensive procedure for the fabrication of structural color filters at ambient conditions and $T \leq 50$ °C using electrodeposition of gold (Au) and cuprous oxide (Cu₂O). As a demonstration, electrodeposition of tri-layer asymmetric metal/dielectric/metal (MDM) Fabry-Pérot (F-P) cavities is shown, producing bright reflective colors. Here, we constrain the thickness of both the top thin and the bottom Au films and adjust solely the thickness of the Cu₂O layers to obtain different colors of high brightness. Unlike simple structural color films based upon uncapped oxide films,³⁴⁻³⁶ the MDM structures demonstrated here show several fundamental and practical advantages. First, due to the high refractive index of Cu₂O, the color of the resultant electrodeposited MDM films is angle-insensitive at viewing angles up to ± 60 °. Second, the electrodeposition method shown here produces MDM structural colors across the CMY color space with superior brightness. In fact, the successful electrodeposition of uniformly thin metal layers on a dielectric substrate over macroscopic dimensions, which directly results into the high brightness of generated colors, is one of the primary achievements in this work. Third, the electrodeposition process is comparatively rapid, performed without expensive

ancillary process equipment, and compatible with irregular, curved substrates. Specifically, a fully aqueous, non-toxic electrolyte is utilized that is free of any harmful pollutants. Fourth, the films are strongly adherent on stainless steel substrates. The suitability of the presented electrodeposition strategy to prepare **structural colors and directly on arbitrary size and shaped conductive surfaces**, with the capacity for scaling up is discussed. This facile and inexpensive method may potentially lead to extensive uses of structural colors in diverse applications, including solar cells, color displays, and aesthetic decorations, at a lower cost.

Results and Discussion

Figure 1a illustrates **the schematic of the electrodeposition process for layered optical films in the form of Au/Cu₂O/Au tri-layer MDM stacks deposited on a heavily n-doped crystalline silicon (Si) substrate**. The electrodeposition was performed using a standard **three-electrode electrochemical cell design (Figure 1b)**. Here the conductive n⁺-Si substrates and a platinum mesh were used as the working and counter electrodes, respectively, while **suitable reference electrodes were used for the three-electrode electrochemical cell setup**. Further details on **the setup** are listed in the Methods Section. For electrodeposition of MDM structural colors on flat surfaces, hydrogen-terminated crystalline n⁺-Si (111) substrates with a small miscut angle ($\pm 0.5^\circ$) were specifically employed to improve the uniformity of the first Au layer.³⁷

The thicknesses **of the bottom Au reflector was 40 nm, while the top Au layer was set to 15 nm**. Different colors can be obtained by varying the Cu₂O cavity layer

thickness, which determines the F-P cavity resonances to enhance the absorption by the top Au layer at discrete wavelengths. For example, pure cyan, magenta, and yellow (CMY) film colors were realized with electrodeposited Cu₂O thicknesses of 70, 45, and 20 nm, respectively. The measured reflectance spectra in Figure 1c (dashed curves) of the CMY colored devices agreed very well with predictions from optical simulations of the respective MDM structures (solid curves) based on the transfer matrix method³⁸ with the refractive indices and thicknesses of electrodeposited Au and Cu₂O layers determined by spectroscopic ellipsometry. The insets in Figure 1c illustrate the colors of the fabricated devices as viewed from 0° with respect to the surface normal.

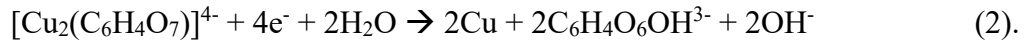
Figure 2a shows the refractive indices n and k (the real and imaginary parts of the refractive index, respectively) of the electrodeposited Au and Cu₂O films. Both data sets are generally in agreement with data recorded for Au and Cu₂O films prepared by vacuum-based deposition methods. The refractive index of the reference Au was characterized using Au films grown in our own lab by e-beam evaporation and the reference data for reactively-sputtered Cu₂O was extracted from Ref. [39]. Accordingly, these measurements illustrate the high quality optical properties of these films despite being prepared entirely from aqueous solution. Even the measurably smaller n for electrodeposited Cu₂O as compared to that for Cu₂O bulk standards resulted in the need for only slightly thicker Cu₂O layers to generate a reflectance dip at a given wavelength and to realize functional cavity layers for a given color. Figure 2b provides the net phase shift calculated using the measured refractive indices, which includes two reflection phases at both the top and bottom interfaces and the

accumulated propagation phase within the Cu₂O layer for the three CMY MDM films. These data clearly indicate the absorption resonances ($\lambda=458$ nm for yellow, $\lambda=531$ nm for magenta, and $\lambda=618$ nm for cyan, where the net phase shift is equal to a multiple of 2π) that selectively absorb light in the visible range for the reflective color generation, and are in agreement with the reflectance dips seen in Figure 1c.

Since high smoothness and uniformity are required to obtain highly reflective structural colors, appropriate care must be taken to ensure low surface roughness of these electrodeposited films. The first Au layer was deposited following an approach developed for electrodeposition of flat Au on Si(111) with an aqueous solution containing 0.1 mM HAuCl₄·3H₂O, 1 mM KCl, 1 mM H₂SO₄ and 100 mM K₂SO₄,⁴⁰ adapted following separate reports suggesting lower electrodeposition roughness with Si (111) substrates with small miscut angles.^{37, 41, 42} Electrodeposition of this Au layer was performed potentiostatically at $E = -1.9$ V vs. $E(\text{Ag}/\text{AgCl})$. Au film growth rates of ~ 1 nm min⁻¹ were determined from the as-deposited films using spectroscopic ellipsometry and cross-sectional scanning electron microscopy (SEM). Faster growth rates at this potential were possible by increasing the concentration of HAuCl₄·3H₂O if the pH was separately maintained. Figure 3a shows atomic force microscopy (AFM) measurements of a 40 nm thick Au film uniformly electrodeposited on a n⁺-Si(111) substrate. The root-mean-square roughness (R_{RMS}) was measured to be ~ 1.4 nm.

The electrodeposition of Cu₂O on these Au films was performed galvanostatically in an alkaline solution where Cu(II) hydroxypropane-1,2,3-tricarboxylate (i.e. copper citrate) was generated by addition of 0.4 M CuSO₄·5H₂O and 1.6 M citric acid

(H₃C₆H₄O₆OH).⁴³ The applied cathodic current density, *j*, dictated whether Cu₂O (*j* = 0.1 mA cm⁻²) or Cu (*j* ≥ 1 mA cm⁻²) was produced,⁴⁴



Care was taken to avoid producing any Cu⁰ in the Cu₂O films. A solution temperature of 50 °C and *pH* – 10.9 were employed. Cu₂O electrodeposition rates ranging from 0.05 – 0.1 nm s⁻¹ were observed. Representative chronopotentiometry plots for three different thicknesses of electrodeposited Cu₂O are presented in the Supporting Information (Figure S1), highlighting both the repeatability of electrodepositions and the ability to readily use time as the sole variable to determine thickness. AFM measurements of a 45 nm thick Cu₂O film (used for the magenta device) electrodeposited on the same Au film in Figure 3a are shown in Figure 3b. The *R_{RMS}* was slightly larger (4.2 nm) but nonetheless more than low enough to maintain a mirror-like appearance.

The electrodeposition of a thin metal layer of good optical quality on top of a dielectric was the most challenging. For example, the intent to use the same bath for the Cu₂O electrodeposition and just grow a capping Cu⁰ layer^{43, 45-48} failed to produce smooth Cu with good optical property (details see Figure S2). Electrodeposition of the top metal layer required satisfying several constraints: uniformity over large areas while maintaining minimal thickness (i.e. < 20 nm), low surface roughness to avoid deleterious light scattering effects, and not compromising the physical and chemical integrity of the underlying Cu₂O. Specifically, either chemical etching of Cu₂O or

partial reduction of Cu sites that perturbs film stoichiometry during top metal electrodeposition would compromise the optical quality of the MDM structures. As an alternative, Au films were again electrodeposited using the same stock solution that was prepared for the bottom Au electrodeposition, however a radically different methodology than that used for the underlying Au film was necessary. Cu₂O is more chemically stable in alkaline solutions and will not reduce to Cu⁰ so long as the potential is not made more negative than approximately -0.5 V vs. $E(\text{Ag}/\text{AgCl})$ (for $p\text{H} \sim 11$).⁴⁹ For these reasons, the $p\text{H}$ of the stock solution was increased to ~ 10 -11. In this solution at $T = 50$ °C, Au electrodeposition was possible over a wide potential range ($-2.06 < E < -0.52$ V vs. $E(\text{Ag}/\text{AgCl})$). Still, electrodepositions performed at $E < -1.05$ V vs. $E(\text{Ag}/\text{AgCl})$ on the Au/Cu₂O MD stack resulted in peeling off due to H₂ bubbles from concurrent proton reduction process. Accordingly, the top Au layer was specifically electrodeposited at $E = -0.52$ V vs. $E(\text{Ag}/\text{AgCl})$ and $T = 50$ °C with constant solution convection. These factors ensured the underlying Cu₂O films were not compromised. AFM measurements of the final MDM structures are provided in Figure 3c. The overall roughness of the MDM stack is not significantly increased on electrodeposition of the 15 nm thick top Au film, as can be seen from the R_{RMS} (= 5.3 nm) and R_a (= 3.5 nm) values. Although some larger Au aggregates (100 nm wide, 30 nm thick) suggestive of sporadic 3D film growth were observed, the overall macroscopic uniformity and regularity of these films yielded reflectance spectra very similar to responses predicted for the ideal flat slab film stacks (Figure 1). The SEM image in Figure 3d presents a cross-section image of a magenta colored MDM stack. The average thickness of the

individual layers in this tri-layer stack match the intended thicknesses for each layer that were optimized using optical simulations. Both the small degree of thickness variation during electrodeposition and the surface roughness of electrodeposited films lead to the slight discrepancy between the measured and simulated reflectance spectra as seen in Figure 1c.

The angle-resolved reflectance for electrodeposited Au/Cu₂O/Au MDM stacks measured using unpolarized light are presented in Figures 4a-c. The measured spectra agree well with the model predictions for the angle-resolved reflectance of ideal Au/Cu₂O/Au MDM stacks shown in Figures 4d-f. Owing to the high refractive index of the Cu₂O cavity layer which elicits a very small refracted angle into the structure, the reflectance minima for the CMY colors are independent of the incident angle up to $\pm 60^\circ$.^{6, 10, 50} Figure 4g presents a set of electrodeposited CMY structural color films viewed at various angles under ambient white light. In these images, the color purity of the films is unchanged at the different viewing angles, which addresses one of the key challenges facing many structural color designs.^{17, 51-53}

A final test of the unique merits of electrodeposition as methodology for MDM color films was carried out on an irregularly shaped substrate. When performed carefully, electrodeposition can yield films that follow closely the contours of any electrode shape. To demonstrate the control afforded by the cumulative process developed here, Au/Cu₂O/Au MDM stacks were deposited on a working electrode consisting of stainless-steel spoons. Figure 5 shows the resultant glossy and uniform color appearance of CMY colors on the curved and rough surfaces of these spoons. In

these images, the curved profile of the spoon in effect illustrates reflectance over a wide range of viewing angles. The homogeneity and consistency of the colors, in addition to the lustrous appearance, directly validate the electrodeposited MDM approach and the great uniformity in thickness of each electrodeposited layer. The uniformity of the electrodeposited films is discussed further in the Supporting Information (Figure S3). In addition, a further advantage of these electrodeposited MDM films was noted in an adhesion test. A standard peel test using adhesive tape⁵⁴ was applied on the as-prepared MDM coatings. These MDM films remained strongly adhered to stainless steel without obvious mechanical damage.

A final note should be made regarding the specific components employed here. n+-doped Si was used in this study for easy cleaving of the sample for SEM characterization. Many other substrates can be used, as long as a conductive seed layer is provided. In principle, electrodeposition of MDM layers can be performed with a wide variety of different metal and dielectric layers. The Cu₂O dielectric layer represents a significant improvement in terms of safety over prior demonstrations of electrodeposited structural colors. Specifically, electrodeposited chromium oxide films have been used as interference color coatings on metal surfaces^{34, 36, 55, 56} because film thicknesses up to 500 nm can be readily obtained.^{57, 58} However, the toxicity of chromium electrolytes is substantial and such solutions are considered extremely potent pollutants.⁵⁹ In contrast, the copper citrate solution used here is comparatively benign, closely mirroring the composition of a common colorimetric solution used to test for sugars in water.⁶⁰ Still, it is conceivable that other dielectrics that can be readily

electrodeposited including amorphous silicon,⁶¹ titanium oxide,⁶² and zinc oxide⁶³ could be used to form cavity layers in MDM structures. Doing so may facilitate the electrodeposition of other coinage metals such as Ag, Cu, and Al that would lead to similar reflectance and brightness properties.

Conclusions

In summary, we have demonstrated a novel and simple approach for generating MDM structural color films that can be performed entirely under ambient pressure and temperature conditions using a facile bench-top electrochemical set up. These structural colors are designed based on tri-layer MDM Fabry-Pérot resonators. The cavity layer (Cu_2O) thickness was readily tuned by electrodeposition parameters so as to generate any arbitrary CMY color. The electrodeposited films exhibit stable and angle-insensitive color, owing to the high refractive index of electrodeposited Cu_2O . These MDM films were strongly adherent as-prepared. This electrodeposition tactic was applied both to flat and curved substrates and is readily scalable since expensive ancillary equipment is not required. These aspects cumulatively open up new avenues for development and implementation MDM structural color films.

Methods

Chemicals and Materials. Acetone (ACS grade, Fisher Scientific), methanol (ACS grade, Fisher Scientific), 2-propanol (ACS grade, Fisher Scientific), buffered hydrofluoric acid (BHF, Transene Inc.), 49% hydrofluoric acid (HF, Transene Inc.), gold (III) chloride

trihydrate ($\text{HAuCl}_4 \cdot 3\text{H}_2\text{O}$, >99.9% Sigma-Aldrich), potassium sulfate (K_2SO_4 , ACS grade, Fisher Scientific), potassium chloride (KCl , ACS grade, Fisher Scientific), sulfuric acid (H_2SO_4 , 0.1 M eluent concentrate for IC, Sigma-Aldrich), copper (II) sulfate pentahydrate ($\text{CuSO}_4 \cdot 5\text{H}_2\text{O}$, ACS grade, Avantor), citric acid (>99.5% ACS grade, Sigma-Aldrich), sodium hydroxide (NaOH , >98% ACS grade, Sigma-Aldrich), indium (99.99%, Gallium Source), and gallium (99.999%, Alfa Aesar) were used as received. Degenerately doped n^+ - $\text{Si}(111)$ wafers with $a \pm 0.5^\circ$ miscut (0.525 ± 0.020 mm, $\rho < 0.007 \Omega \cdot \text{cm}$, Addison Engineering, Inc.) were diced and used as substrates. Deionized (DI) water with a resistivity $> 18.2 \text{ M}\Omega \cdot \text{cm}$ was used throughout.

Substrate preparation. Both n^+ - $\text{Si}(111)$ substrates and stainless-steel spoons were degreased by sequentially sonicating for five minutes each in acetone, methanol, isopropyl alcohol, and water, and then dried under a nitrogen (N_2) gas stream. H-terminated $\text{Si}(111)$ surfaces were prepared by immersion of the Si substrates in 5% HF for 30 seconds, soaking in DI water at $T = 95^\circ\text{C}$ for 20 minutes, and then etching sequentially in 5% HF and BHF for 30 seconds each. Etched Si substrates were then rinsed with water, dried under a $\text{N}_2(\text{g})$ stream, and were immediately used for the electrodepositions. The stainless-steel spoons were used as working electrodes directly after the initial degreasing steps without any HF etch steps.

Electrodeposition of Au and Cu_2O . All electrochemical depositions were performed in a three-electrode cell in lab ambient and $T \leq 50^\circ\text{C}$. Computer controlled

potentiostats (CHI760C, CH Instruments and Solartron Analytical 1287A, AMETEK Scientific Instruments) were used throughout. A platinum mesh counter electrode was used for all electrodepositions whereas multiple reference electrodes were employed as dictated by the *pH* of the electrodeposition solution.

An aqueous stock solution of 0.1 mM $\text{HAuCl}_4 \cdot 3\text{H}_2\text{O}$, 1 mM KCl, and 100 mM K_2SO_4 was prepared for Au electrodeposition. For the bottom Au film, a portion of this stock solution was separated and 1 mM H_2SO_4 was added to it to adjust the *pH* to ~ 3 .³⁷,⁴⁰ An aqueous Ag/AgCl (sat. KCl) electrode was employed as the reference electrode for these solutions. Ohmic contact to the Si substrate was made by applying eutectic gallium-indium to the tip of the wafer and clipping the working electrode of the potentiostat to this region. For the case of stainless-steel spoons, the working electrode of the potentiostat was directly clipped on to the end of the spoon. The Si substrate was prepolarized by applying a potential of $E = -1.9$ V vs. $E(\text{Ag/AgCl})$ and was then immersed into solution. This prepolarization step was necessary to avoid electroless plating of Au and the formation of a native oxide layer on Si that could prevent further epitaxial Au growth. A potential of $E = -1.45$ V vs. $E(\text{Ag/AgCl})$ was selected for Au electrodeposition on the spoons in order to avoid excessive hydrogen evolution at more negative potentials (Figure S4). For all samples, electrodepositions performed for 40 minutes at $T = 35$ °C with a stirred solution yielded uniform ~ 40 nm thick Au films.

Cu_2O was electrodeposited from alkaline Cu(II)-citrate solutions, as has been demonstrated previously.⁴³ An aqueous solution of 0.4 M $\text{CuSO}_4 \cdot 5\text{H}_2\text{O}$ and 1.6 M citric acid was prepared and NaOH was slowly added to this solution to raise the *pH* to ~ 10.9 .

A mercury sulfate (sat. K_2SO_4) electrode was employed as the reference electrode in the three-electrode cell, but all stated potentials are reported with respect to $E(\text{Ag}/\text{AgCl})$. Kapton tape was used to define the total active area of these working electrodes in contact with the solution. The cathodic current density during the electrodeposition was tuned between 0.05 to 0.1 mA cm^{-2} to ensure the potential measured during electrodeposition did not exceed $E = -0.41 \text{ V}$ vs. $E(\text{Ag}/\text{AgCl})$. Electrodepositions performed at $T = 50 \text{ }^\circ\text{C}$ and under convection resulted in uniform Cu_2O electrodeposition ($\sim 0.05 - 0.1 \text{ nm s}^{-1}$) and a measured potential of $E = -0.16 \text{ V}$ to -0.41 V vs. $E(\text{Ag}/\text{AgCl})$.

For the electrodeposition of the top Au layer, an alkaline solution was utilized to prevent compromising the Cu_2O layer. A portion of the stock Au solution prepared above was separated and its pH was adjusted to $\sim 10-11$ by addition of NaOH. A mercury sulfate (sat. K_2SO_4) reference electrode was employed. Top Au layers with thicknesses of approximately 15 nm were electrodeposited at $E = -0.52 \text{ V}$ vs. $E(\text{Ag}/\text{AgCl})$ at $T = 50 \text{ }^\circ\text{C}$ under convection for 30 minutes.

Optical Simulations. Simulated reflectance spectra and the net phase shifts within the Cu_2O layer were calculated based on the transfer matrix method.³⁸ These simulations used measured refractive indices from a spectroscopic ellipsometer (M-2000, J. A. Woollam Co.) as inputs.

MDM film characterization. Reflectance spectra at normal incidence were measured using a thin-film measurement instrument (F20, Filmetrics) integrated with a spectrometer and a white light source. Angle-resolved reflectance spectra of as-prepared MDM stacks and determination of the thickness of each layer were performed with a spectroscopic ellipsometer (M-2000, J. A. Woollam Co.). The smallest incident angle measurable with this instrument was 45°. Thus, the measured spectra in Figure 4 has an angular range of 45° to 60°. Reflectance spectra simulations for 0° to 60° viewing angles are reported to illustrate the wide range of angle insensitivity for our structural colors (Figure 4d-f). Cross-sectional scanning electron microscopy was performed with a SU8000 FE-SEM (Hitachi High-Technologies Corporation) with a Schottky field emitter operated at 5 keV beam voltage. The surface morphology of each layer was investigated by tapping mode atomic force microscopy (TESPA-V2 tip and Dimension Icon AFM, Bruker Corporation).

Supporting Information

The Supporting Information is available free of charge on the ACS Publications website at DOI:

Chronopotentiometry Plots for Cu₂O electrodeposition; Issues Related to Electrodeposited Cu; Thickness Uniformity of Electrodeposited Films; Cyclic Voltammetry response for Si and stainless-steel spoon electrode in Au electrodeposition solution

Author Information

Corresponding Author

*Email (S. M.): smald@umich.edu

*Email (L. J. G.): guo@umich.edu

ORCID

Chengang Ji: 0000-0002-6658-9853

Saurabh Acharya: 0000-0002-2855-457X

Kaito Yamada: 0000-0003-4413-6340

Stephen Maldonado: 0000-0002-2917-4851

L. Jay Guo: 0000-0002-0347-6309

Author Contributions

[†]C. J. and S. A. contributed equally to this work

Acknowledgements

This work is supported in part by the National Science Foundation (CMMI-1727918).

S. M. recognizes the National Science Foundation (CHE1505635) for partial support of this work.

References

1. Arsenault, A. C.; Puzzo, D. P.; Manners, I.; Ozin, G. A., Photonic-Crystal Full-Colour Displays. *Nat. Photon.* **2007**, *1*, 468-472.
2. Hong, J.; Chan, E.; Chang, T.; Fung, T.-C.; Hong, B.; Kim, C.; Ma, J.; Pan, Y.; Lier, R. V.; Wang, S.-g.; Wen, B.; Zhou, L., Continuous Color Reflective Displays Using Interferometric Absorption. *Optica* **2015**, *2*, 589-597.
3. Zhu, X.; Vannahme, C.; Højlund-Nielsen, E.; Mortensen, N. A.; Kristensen, A., Plasmonic Colour Laser Printing. *Nat. Nanotechnol.* **2016**, *11*, 325-329.
4. Kumar, K.; Duan, H.; Hegde, R. S.; Koh, S. C. W.; Wei, J. N.; Yang, J. K. W., Printing Colour at the Optical Diffraction Limit. *Nat. Nanotechnol.* **2012**, *7*, 557-561.
5. Kim, H.; Ge, J.; Kim, J.; Choi, S.-e.; Lee, H.; Lee, H.; Park, W.; Yin, Y.; Kwon, S., Structural Colour Printing Using a Magnetically Tunable and Lithographically Fixable Photonic Crystal. *Nat. Photon.* **2009**, *3*, 534-540.
6. Lee, K.-T.; Ji, C.; Banerjee, D.; Guo, L. J., Angular- and Polarization-Independent

Structural Colors Based on 1D Photonic Crystals. *Laser Photon. Rev.* **2015**, *9*, 354-362.

7. Banerjee, D.; Zhang, M., Quarter-Wave Design Criteria for Omnidirectional Structural Colors. *J. Mod. Opt.* **2010**, *57*, 1180-1188.

8. Masuda, T.; Kudo, Y.; Banerjee, D., Visually Attractive and High-Power-Retention Solar Modules by Coloring with Automotive Paints. *Coatings* **2018**, *8*, 282.

9. Masuda, T.; Hirai, S.; Inoue, M.; Chantana, J.; Kudo, Y.; Minemoto, T., Colorful, Flexible, and Lightweight Cu(In,Ga)Se₂ Solar Cell by Lift-Off Process with Automotive Painting. *IEEE J. Photovolt.* **2018**, *8*, 1326-1330.

10. Ji, C.; Lee, K.-T.; Xu, T.; Zhou, J.; Park, H. J.; Guo, L. J., Engineering Light at the Nanoscale: Structural Color Filters and Broadband Perfect Absorbers. *Adv. Opt. Mater.* **2017**, *5*, 1700368.

11. Xu, G.; Shen, L.; Cui, C.; Wen, S.; Xue, R.; Chen, W.; Chen, H.; Zhang, J.; Li, H.; Li, Y.; Li, Y., High-Performance Colorful Semitransparent Polymer Solar Cells with Ultrathin Hybrid-Metal Electrodes and Fine-Tuned Dielectric Mirrors. *Adv. Funct. Mater.* **2017**, *27*, 1605908.

12. Lu, J.-H.; Lin, Y.-H.; Jiang, B.-H.; Yeh, C.-H.; Kao, J.-C.; Chen, C.-P., Microcavity Structure Provides High-Performance (>8.1%) Semitransparent and Colorful Organic Photovoltaics. *Adv. Funct. Mater.* **2017**, *28*, 1703398.

13. Ji, C.; Zhang, Z.; Masuda, T.; Kudo, Y.; Guo, L. J., Vivid-Colored Silicon Solar Panels with High Efficiency and Non-Iridescent Appearance. *Nanoscale Horiz.* **2019**, *4*, 874-880.

14. Sabnis, R. W., Color Filter Technology for Liquid Crystal Displays. *Displays* **1999**, *20*, 119-129.

15. Xu, T.; Wu, Y.-K.; Luo, X.; Guo, L. J., Plasmonic Nanoresonators for High-Resolution Colour Filtering and Spectral Imaging. *Nat. Commun.* **2010**, *1*, 59.

16. Davis, M. S.; Zhu, W.; Xu, T.; Lee, J. K.; Lezec, H. J.; Agrawal, A., Aperiodic Nanoplasmonic Devices for Directional Colour Filtering and Sensing. *Nat. Commun.* **2017**, *8*, 1347.

17. Uddin, M. J.; Magnusson, R., Highly Efficient Color Filter Array Using Resonant Si₃N₄ Gratings. *Opt. Express* **2013**, *21*, 12495-12506.

18. Kaplan, A. F.; Xu, T.; Guo, L. J., High Efficiency Resonance-Based Spectrum Filters with Tunable Transmission Bandwidth Fabricated Using Nanoimprint Lithography. *Appl. Phys. Lett.* **2011**, *99*, 143111.

19. Li, Z.; Butun, S.; Aydin, K., Large-Area, Lithography-Free Super Absorbers and Color Filters at Visible Frequencies Using Ultrathin Metallic Films. *ACS Photonics* **2015**, *2*, 183-188.

20. Yang, C.; Shen, W.; Zhang, Y.; Li, K.; Fang, X.; Zhang, X.; Liu, X., Compact Multilayer Film Structure for Angle Insensitive Color Filtering. *Sci. Rep.* **2015**, *5*, 9285.

21. Park, C.-S.; Shrestha, V. R.; Lee, S.-S.; Choi, D.-Y., Trans-Reflective Color Filters based on a Phase Compensated Etalon Enabling Adjustable Color Saturation. *Sci. Rep.* **2016**, *6*, 25496.

22. <https://www.youtube.com/watch?v=nYu1ruSakRg&t=128s>.

23. Xiao, M.; Li, Y.; Allen, M. C.; Deheyn, D. D.; Yue, X.; Zhao, J.; Gianneschi, N. C.; Shawkey, M. D.; Dhinojwala, A., Bio-Inspired Structural Colors Produced via Self-

Assembly of Synthetic Melanin Nanoparticles. *ACS Nano* **2015**, *9*, 5454-5460.

- 24. Mihi, A.; Ocaña, M.; Míguez, H., Oriented Colloidal-Crystal Thin Films by Spin-Coating Microspheres Dispersed in Volatile Media. *Adv. Mater.* **2006**, *18*, 2244-2249.
- 25. Gao, W.; Rigout, M.; Owens, H., Self-Assembly of Silica Colloidal Crystal Thin Films with Tuneable Structural Colours over a Wide Visible Spectrum. *Appl. Surf. Sci.* **2016**, *380*, 12-15.
- 26. Shim, T. S.; Kim, S.-H.; Sim, J. Y.; Lim, J.-M.; Yang, S.-M., Dynamic Modulation of Photonic Bandgaps in Crystalline Colloidal Arrays Under Electric Field. *Adv. Mater.* **2010**, *22*, 4494-4498.
- 27. Park, J.-G.; Benjamin Rogers, W.; Magkiriadou, S.; Kodger, T.; Kim, S.-H.; Kim, Y.-S.; Manoharan, V. N., Photonic-Crystal Hydrogels with a Rapidly Tunable Stop Band and High Reflectivity across the Visible. *Opt. Mater. Express* **2017**, *7*, 253-263.
- 28. Li, F.; Tang, B.; Zhang, S., Iridescent Structural Colors from Self-Assembled Polymer Opal of Polythiourethane Microspheres. *Dyes Pigm.* **2017**, *142*, 371-378.
- 29. Josell, D.; Wheeler, D.; Huber, W. H.; Moffat, T. P., Superconformal Electrodeposition in Submicron Features. *Phys. Rev. Lett.* **2001**, *87*, 016102.
- 30. Ozel, T.; Zhang, B. A.; Gao, R.; Day, R. W.; Lieber, C. M.; Nocera, D. G., Electrochemical Deposition of Conformal and Functional Layers on High Aspect Ratio Silicon Micro/Nanowires. *Nano. Lett.* **2017**, *17*, 4502-4507.
- 31. Inoue, F.; Harada, Y.; Koyanagi, M.; Fukushima, T.; Yamamoto, K.; Tanaka, S.; Wang, Z.; Shingubara, S., Perfect Conformal Deposition of Electroless Cu for High Aspect Ratio Through-Si Vias. *Electrochem. Solid-State Lett.* **2009**, *12*, H381-H384.
- 32. Gunawardena, G.; Hills, G.; Montenegro, I.; Scharifker, B., Electrochemical Nucleation: Part I. General Considerations. *J. Electroanal. Chem. Interfacial Electrochem.* **1982**, *138*, 225-239.
- 33. Gunawardena, G.; Hills, G.; Montenegro, I., Electrochemical Nucleation: Part II. The Electrodeposition of Silver on Vitreous Carbon. *J. Electroanal. Chem. Interfacial Electrochem.* **1982**, *138*, 241-254.
- 34. Hoeckelman, R. F., Optical Properties of Chromium-Plated Steel. *J. Electrochem. Soc.* **1972**, *119*, 1310-1315.
- 35. Fredj, N.; Burleigh, T. D., Transpassive Dissolution of Copper and Rapid Formation of Brilliant Colored Copper Oxide Films. *J. Electrochem. Soc.* **2011**, *158*, C104-C110.
- 36. Ogura, K.; Lou, W.; Nakayama, M., Coloration of Stainless Steel at Room Temperature by Triangular Current Scan Method. *Electrochim. Acta* **1996**, *41*, 2849-2853.
- 37. Prod'homme, P.; Maroun, F.; Cortès, R.; Allongue, P., Electrochemical Growth of Ultraflat Au(111) Epitaxial Buffer Layers on H-Si(111). *Appl. Phys. Lett.* **2008**, *93*, 171901.
- 38. Petterson, L. A. A.; Roman, L. S.; Inganäs, O., Modeling Photocurrent Action Spectra of Photovoltaic Devices based on Organic Thin Films. *J. Appl. Phys.* **1999**, *86*, 487-496.
- 39. Drobny, V. F.; Pulfrey, L., Properties of Reactively-Sputtered Copper Oxide Thin Films. *Thin Solid Films* **1979**, *61*, 89-98.
- 40. Mahenderkar, N. K.; Chen, Q.; Liu, Y.-C.; Duchild, A. R.; Hofheins, S.; Chason, E.;

Switzer, J. A., Epitaxial Lift-Off of Electrodeposited Single-Crystal Gold Foils for Flexible Electronics. *Science* **2017**, *355*, 1203-1206.

41. Prodhomme, P.; Warren, S.; Cortès, R.; Jurca, H. F.; Maroun, F.; Allongue, P., Epitaxial Growth of Gold on H-Si(111): The Determining Role of Hydrogen Evolution. *Chemphyschem* **2010**, *11*, 2992-3001.

42. Switzer, J. A.; Hill, J. C.; Mahenderkar, N. K.; Liu, Y.-C., Nanometer-Thick Gold on Silicon as a Proxy for Single-Crystal Gold for the Electrodeposition of Epitaxial Cuprous Oxide Thin Films. *ACS Appl. Mater. Interfaces* **2016**, *8*, 15828-15837.

43. Eskhult, J.; Nyholm, L., Pulsed Galvanostatic and Potentiostatic Electrodeposition of Cu and Cu₂O Nanolayers from Alkaline Cu(II)-Citrate Solutions. *J. Electrochem. Soc.* **2008**, *155*, D115-D122.

44. Eskhult, J.; Herranen, M.; Nyholm, L., On the Origin of the Spontaneous Potential Oscillations Observed during Galvanostatic Deposition of Layers of Cu and Cu₂O in Alkaline Citrate Solutions. *J. Electroanal. Chem.* **2006**, *594*, 35-49.

45. Switzer, J. A.; Hung, C.-J.; Huang, L.-Y.; Miller, F. S.; Zhou, Y.; Raub, E. R.; Shumsky, M. G.; Bohannan, E. W., Potential Oscillations during the Electrochemical Self-Assembly of Copper/Cuprous Oxide Layered Nanostructures. *J. Mater. Res.* **2011**, *13*, 909-916.

46. Switzer, J. A.; Hung, C.-J.; Huang, L.-Y.; Switzer, E. R.; Kammler, D. R.; Golden, T. D.; Bohannan, E. W., Electrochemical Self-Assembly of Copper/Cuprous Oxide Layered Nanostructures. *J. Am. Chem. Soc.* **1998**, *120*, 3530-3531.

47. Bohannan, E. W.; Huang, L.-Y.; Miller, F. S.; Shumsky, M. G.; Switzer, J. A., In Situ Electrochemical Quartz Crystal Microbalance Study of Potential Oscillations during the Electrodeposition of Cu/Cu₂O Layered Nanostructures. *Langmuir* **1999**, *15*, 813-818.

48. Mishina, E. D.; Nagai, K.; Nakabayashi, S., Self-Assembled Cu/Cu₂O Multilayers: Deposition, Structure and Optical Properties. *Nano. Lett.* **2001**, *1*, 401-404.

49. Beverskog, B.; Puigdomenech, I., Revised Pourbaix Diagrams for Copper at 25 to 300°C. *J. Electrochem. Soc.* **1997**, *144*, 3476-3483.

50. Ji, C.; Lee, K.-T.; Guo, L. J., High-Color-Purity, Angle-Invariant, and Bidirectional Structural Colors based on Higher-Order Resonances. *Opt. Lett.* **2019**, *44*, 86-89.

51. Zulian, L.; Emilitri, E.; Scavia, G.; Botta, C.; Colombo, M.; Destri, S., Structural Iridescent Tuned Colors from Self-Assembled Polymer Opal Surfaces. *ACS Appl. Mater. Interfaces* **2012**, *4*, 6071-6079.

52. Park, H. J.; Xu, T.; Lee, J. Y.; Ledbetter, A.; Guo, L. J., Photonic Color Filters Integrated with Organic Solar Cells for Energy Harvesting. *ACS Nano* **2011**, *5*, 7055-7060.

53. Park, C.-H.; Yoon, Y.-T.; Lee, S.-S., Polarization-Independent Visible Wavelength Filter Incorporating a Symmetric Metal-Dielectric Resonant Structure. *Opt. Express* **2012**, *20*, 23769-23777.

54. Chalker, P. R.; Bull, S. J.; Rickerby, D. S., A Review of the Methods for the Evaluation of Coating-Substrate Adhesion. *Mater. Sci. Eng. A* **1991**, *140*, 583-592.

55. Fujimoto, S.; Shibata, T.; Wada, K.; Tsutae, T., The Electrochemical Conditions for Coloured Film Formation on Type 304 Stainless Steel with Square Wave Polarization.

Corros. Sci. **1993**, *35*, 147-152.

56. Hogg, S. W.; Smith, G. B., The Unusual and Useful Optical Properties of Electrodeposited Chrome-Black Films. *J. Phys. D: Appl. Phys.* **1977**, *10*, 1863-1869.
57. Junqueira, R. M. R.; Loureiro, C. R. d. O.; Andrade, M. S.; Buono, V. T. L., Characterization of Interference Thin Films Grown on Stainless Steel Surface by Alternate Pulse Current in a Sulphochromic Solution. *Mater. Res.* **2008**, *11*, 421-426.
58. Evans, T. E., Film Formation on Stainless Steel in a Solution Containing Chromic and Sulphuric Acids. *Corros. Sci.* **1977**, *17*, 105-124.
59. Sørensen, P. A.; Kiil, S.; Dam-Johansen, K.; Weinell, C. E., Anticorrosive Coatings: A Review. *J. Coat. Technol. Res.* **2009**, *6*, 135-176.
60. Benedict, S. R., A Reagent for the Detection of Reducing Sugars. *J. Biol. Chem.* **1909**, *5*, 485-487.
61. Fulop, G. F.; Taylor, R. M., Electrodeposition of Semiconductors. *Annu. Rev. Mater. Sci.* **1985**, *15*, 197-210.
62. Natarajan, C.; Nogami, G., Cathodic Electrodeposition of Nanocrystalline Titanium Dioxide Thin Films. *J. Electrochem. Soc.* **1996**, *143*, 1547-1550.
63. Lincot, D., Electrodeposition of Semiconductors. *Thin Solid Films* **2005**, *487*, 40-48.

TOC graphic: